Effect of interlayer interactions and lattice distortions on the magnetic ground state and spin dynamics of a geometrically frustrated triangular-lattice antiferromagnet

J. T. Haraldsen and R. S. Fishman

Materials Science and Technology Division, Oak Ridge National Laboratory, Oak Ridge, Tennessee 37831, USA

We investigate the effects of interlayer interactions and lattice distortions on the noncollinear ground state and spin dynamics of a geometrically frustrated triangular-lattice antiferromagnet with implications for the multiferroic phase of doped $CuFeO_2$, where both lattice distortions and anisotropy introduce anharmonic components into the spin ground state. In contrast to the single turn angle of a simple spiral, the turn angles of the predicted ground state are distributed about $\Delta\theta_1$ and $\Delta\theta_2$. Using a Holstein-Primakoff expansion, we show that distinct features in the spin dynamics are associated with the anharmonic components of the spin ground state, which have recently been observed in Ga-doped $CuFeO_2$.

I. INTRODUCTION

The coupling of magnetism and ferroelectricity in multiferroic materials continues to attract attention due to the potential ability to control electric polarization with a magnetic field and magnetic ordering with an electric field.[1–5] Because noncollinear magnetic states are frequently associated with multiferroicity,[5–7] a great deal of work has focused on frustrated magnetic systems.[6] Since ferroelectricity arises in materials with empty d shells whereas magnetism requires partially filled d shells, the coupling between ferroelectricity and ferromagnetism is typically very weak in "proper" multiferroic materials, where magnetism and ferroelectricity reside on different transition-metal sites. Much stronger coupling occurs in "improper" multiferroics, where the electric polarization is induced by the noncollinear ordering of the transition-metal spins.

In most "improper" multiferroics, the electric polarization $\mathbf{P}$ is perpendicular to the chirality $\mathbf{S}_i \times \mathbf{S}_j$ of the spin rotation and the ordering wave vector $\mathbf{Q}$. This multiferroic coupling is explained by the inverse Dzyaloshinskii-Moriya effect within a spin-current model, where inversion symmetry is broken by the chiral magnetic ordering.[1] While this mechanism explains multiferroic behavior in systems that exhibit easy-plane anisotropy, some frustrated magnetic systems with easy-axis anisotropy[4] exhibit a polarization $\mathbf{P}$ parallel to $\mathbf{Q}$. Multiferroic coupling in these materials can be explained by the "spin-driven" model, where $\mathbf{P}$ is produced by the charge transfer created by the metal-ligand hybridization in the presence of spin-orbit coupling.[7] This coupling mechanism is associated with lattice distortions that create triclinic or monoclinic crystal structures. While lower crystal symmetry produces the multiferroic behavior in spin-driven materials, the connection between the lattice distortions and the magnetic structure has not been well understood.

Since geometrically frustrated systems typically have noncollinear magnetic structures and sometimes display multiferroic behavior, they have attracted considerable attention.[8] Ferroelectricity in the geometrically frustrated triangular-lattice antiferromagnet $CuFeO_2$ seems to be described by the spin-driven coupling mechanism. Due to the large spin $S=5/2$ spin of the Fe^{3+} ions, the spin configuration

of $CuFeO_2$ can be evaluated using a semiclassical approximation. At zero field, $CuFeO_2$ has a collinear $\uparrow\uparrow\downarrow\downarrow$ spin configuration. Above a critical magnetic field of ~ 7 T, the spin state becomes noncollinear and multiferroic.[9–12] This multiferroic behavior can be enhanced with either Al or Ga doping,[13–15] which induce a zero-field transition from the $\uparrow\uparrow\downarrow\downarrow$ phase to a complex noncollinear (CNC) phase.[16,17] Multiferroic behavior was observed[18] in Ga-doped $CuFeO_2$ at a Ga concentration of 3.5%.

Based on elastic neutron-scattering (ENS) measurements, Nakajima *et al.*[19,20] proposed that the magnetic ground state of $CuFeO_2$ is the "proper" spiral sketched in Fig. 1(c). This state can be described as a spiral propagating along the $[1,1,0]$ direction with collinear "zigzag" chains in the $[-1,1,0]$ direction. However, Fishman and Okamoto[21] recently demonstrated that the CNC state sketched in Fig. 1(d) is energetically favored over the proper spiral in two dimensions. Due to the presence of anisotropy and lattice distortions, the CNC phase is anharmonic and cannot be approximated by a simple spiral. We recently used a three-dimensional CNC phase[22] to model inelastic neutron-scattering (INS) measurements on 3.5% Ga-doped $CuFeO_2$. The comparison between theoretical predictions and INS measurements confirmed the identification of the multiferroic ground state as the CNC phase and revealed how interlayer coupling, and lattice distortions affect the magnetic ground state and its spin dynamics.

Due to the brevity of the earlier joint theoretical/experimental paper[22] and the possible applications of our theoretical approach to other potential multiferroic materials[23,24] such as $CuCrO_2$ and $MnWO_4$, we will now more clearly explain the method used to evaluate the magnetic ground state and spin dynamics of a geometrically frustrated antiferromagnet. While Fishman and Okamoto[21] investigated the CNC phase for a hexagonal lattice without interlayer interactions, we now show how interlayer interactions affect the spin harmonics and ordering wave vector of the CNC phase. To clarify the magnetic structure of a multiferroic material, we investigate the effects of lattice distortions that break the triangular symmetry of each hexagonal layer. Using the interaction, anisotropy, and lattice distortion parameters required to stabilize the CNC phase[22] in 3.5%
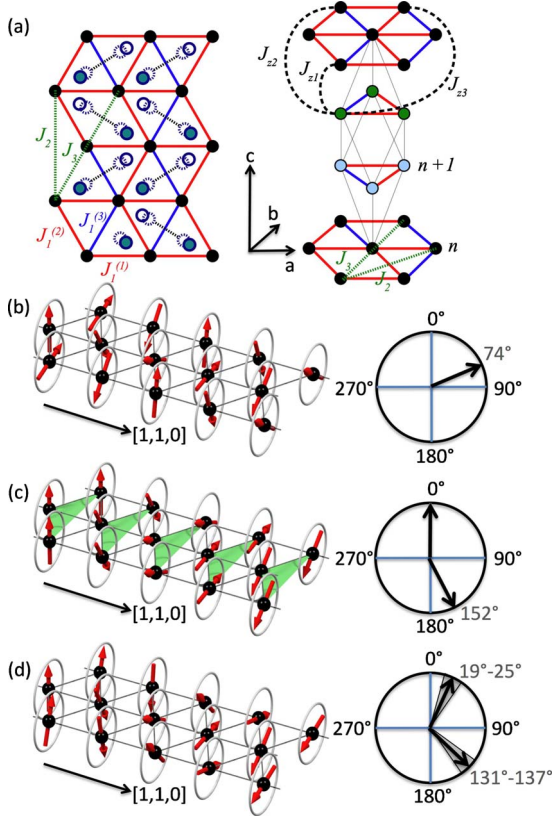
FIG. 1. (Color online) (a) The hexagonal close-packed lattice of the Fe^{3+} ions with intralayer and interlayer interactions. Blue and white atoms indicate oxygen displacement above and below the Fe plane. The magnetic spin configurations of (b) the simple, (c) the proper, and (d) the CNC spirals are sketched with the green triangles in (c) denoting collinear spins. The turn angles for each spin configuration are shown on the right. The CNC phase has a distribution of turn angles clearly shown in Fig. 6(b).

Ga-doped $CuFeO_2$, we compare the evolution of the spin-wave (SW) dynamics of the CNC phase with that of a simple spiral, thereby demonstrating the importance of interlayer interactions and lattice distortions for the spin dynamics of a multiferroic material.

This paper is divided into five sections. Section II describes the formalism used to evaluate the magnetic ground state and spin dynamics. Results for the ground state of the CNC phase are provided in Sec. III and results for the spin dynamics of the simple spiral and CNC phases are provided in Sec. IV. Section V contains a summary.

II. THEORETICAL MODEL WITH LATTICE DISTORTIONS

The hexagonal symmetry of the $CuFeO_2$ lattice provides a complex network of intralayer and interlayer superexchange pathways [see Fig. 1(a)] (Ref. 25) that are described by the Heisenberg Hamiltonian

$$H = -\frac{1}{2}\sum_{i \neq j} J_{ij}\mathbf{S}_i \cdot \mathbf{S}_j - D\sum_i \mathbf{S}_{iz}^2, \qquad (1)$$

where $\mathbf{S}_i$ is the local moment on site i, D is the single-ion anisotropy, and J_{ij} are the exchange couplings between sites

i and j. The exchange interaction is antiferromagnetic when $J_{ij} < 0$. First, second, and third neighbor interactions within and between planes are denoted by J_n and J_{zn}, respectively.

The spin configuration sensitively depends on the isosceles or "scalene" distortion of the triangular lattice associated with the the oxygen displacements[21] sketched in Fig. 1(a). These distortions modulate the nearest-neighbor interactions J_1 [Fig. 1(a)] and break the hexagonal symmetry with $J_1^{(1)} = J_1^{(2)} = J_1 - K_1/2$ and $J_1^{(3)} = J_1 + K_1$. Here, K_1 is a measure of the overall distortion of the lattice. Scalene distortions of the hexagonal layers in $CuFeO_2$ have been observed in both pure[26,27] and Al-doped[28] $CuFeO_2$. The uniform displacement of the oxygen atoms associated with the ferroelectric polarization does not modulate the exchange interactions itself.

To incorporate the spin harmonics of the magnetic ground state, we have modified the classical approach described in Ref. 21 by defining S_z within any hexagonal plane as

$$S_z(\mathbf{R}) = A\left\{ \sum_{l=0} C_{2l+1} \cos[Q_x(2l+1)x] \right.$$
$$\left. + \sum_{l=0} B_{2l+1} \sin[(2\pi - Q_x)(2l+1)x] \right\}, \qquad (2)$$

where the C_{2l+1} harmonics are produced by the anisotropy D and the B_{2l+1} harmonics are produced by the lattice distortion K_1. With C_1 set to 1, the amplitude A is obtained from the condition that the maximum value of $|S_z(\mathbf{R})|$ equals S. Of course, the square of the harmonics are proportional to the observed ENS intensities at odd multiples of Q_x and $2\pi - Q_x$. The perpendicular spin components S_y are given by

$$S_y(\mathbf{R}) = \sqrt{S - S_z(\mathbf{R})^2}\, \text{sgn}[g(\mathbf{R})], \qquad (3)$$

where

$$g(\mathbf{R}) = \sin(Q_x x) + G_1 \cos[(2\pi - Q_x)x], \qquad (4)$$

where G_1 is an additional variational parameter. This parameter only appears when the corresponding B_1 parameter is nonzero and lowers the energy from that evaluated in Ref. 21 in the presence of lattice distortions. In the limit $D \to 0$, $C_{2l+1>1} \to 0$, and $G_1 \to -B_1/C_1$ is required to guarantee rotational symmetry about the x axis. A similar expansion of the spin in powers of the harmonics was obtained to first order in D for a distorted square-lattice antiferromagnet.[29]

The three-dimensional magnetic state is constructed by stacking the two-dimensional configurations antiferromagnetically with a possible lattice shift from one layer to the next. The ordering wave vector Q_x and coefficients C_{2l+1} and B_{2l+1} are determined by minimizing the energy on a large unit cell of size $\sim 10^4 a \times a \times c$, where a is the lattice constant within a hexagonal plane and c is the separation between neighboring planes.

Based on this magnetic ground state, the spin dynamics are evaluated using a Holstein-Primakoff transformation, where the spin operators are given by $S_{iz} = S - a_i^\dagger a_i$, $S_{i+} = \sqrt{2S}a_i$, and $S_{i-} = \sqrt{2S}a_i^\dagger$ (a_i and $a_i^\dagger$ are boson destruction and creation operators). A rotation of the local spin operators accounts for the noncollinearity of the spins.[30,31]

To determine the SW frequencies $\omega_\mathbf{q}$, we solve the equation of motion for the vectors $\mathbf{v_q} = [a_\mathbf{q}^{(1)}, a_\mathbf{q}^{(1)\dagger}, a_\mathbf{q}^{(2)}, a_\mathbf{q}^{(2)\dagger}, \ldots]$,
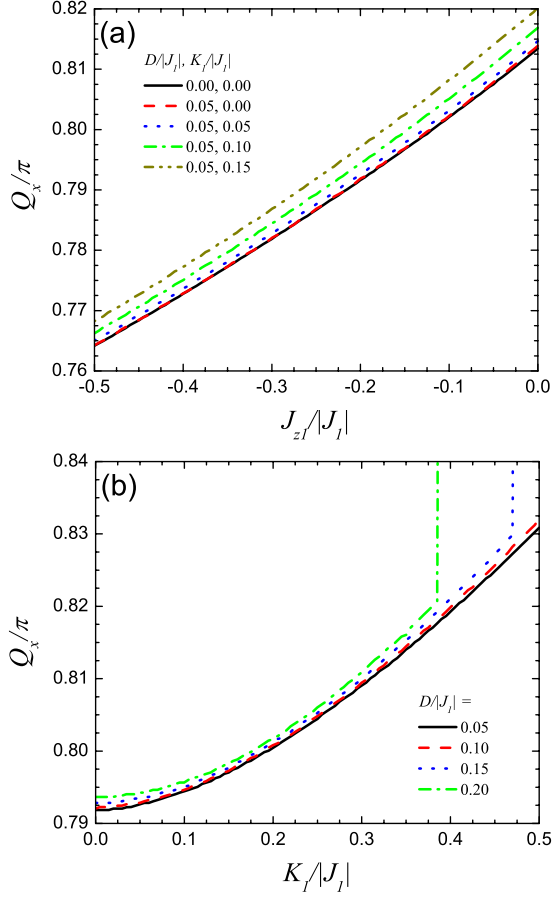
FIG. 2. (Color online) (a) The ordering wave vector as function of J_{z1}/J_1 with various anisotropy and lattice distortion parameters. (b) The ordering wave vector as function of $K_1/|J_1|$ with $J_{z1}/|J_1|=0.2$ and various anisotropy parameters.

FIG. 3. (Color online) (a) The C_3 and C_5 spin harmonics as a function of $D/|J_1|$ with $J_{z1}/|J_1|=-0.2$ and no lattice distortion. (b) The C_3, C_5, B_1, and B_3 spin harmonics as a function of $J_{z1}/|J_1|$ with $D/|J_1|=0.05$ and $K_1/|J_1|=0$ (dark solid lines) and $K_1/|J_1|=0.35$ (light dashed lines).

which may be written in terms of the $2N \times 2N$ matrix $\underline{M}(\mathbf{q})$ as $id\mathbf{v_q}/dt=-[\underline{H}_2,\mathbf{v_q}]=\underline{M}(\mathbf{q})\mathbf{v_q}$, where N is the number of spin sites in the unit cell.[30] The SW frequencies are then determined from the condition $\text{Det}[\underline{M}(\mathbf{q})-\omega_{\mathbf{q}}\underline{I}]=0$. To assure the local stability of a magnetic phase, all SW frequencies must be real and positive and all SW weights must be positive.

The SW intensities or weights are coefficients of the spin-spin correlation function

$$S(\mathbf{q},\omega)=\sum_{\alpha\beta}(\delta_{\alpha\beta}-q_\alpha q_\beta)S^{\alpha\beta}(\mathbf{q},\omega), \qquad (5)$$

where α and β are x, y, or z.[32] A more detailed discussion of this method is contained in Ref. 30. Notice that INS measurements only detect components of the spin fluctuations perpendicular[33] to the wave vector $\mathbf{q}$.

The total intensity $I(\mathbf{q},\omega)$ for an INS scan at constant $\mathbf{q}$ is given by

$$I(\mathbf{q},\omega)=S(\mathbf{q},\omega)F_{\mathbf{q}}^2\exp[-(\omega-\omega_{\mathbf{q}})^2/2\delta^2], \qquad (6)$$

where δ is the energy resolution and $F_{\mathbf{q}}$ is the Fe^{3+} ionic form factor.[34,35] The simulated energy resolution is based on a Gaussian distribution, which is standard for constant $\mathbf{q}$ scans on a triple-axis spectrometer.[33,36] Other experimental
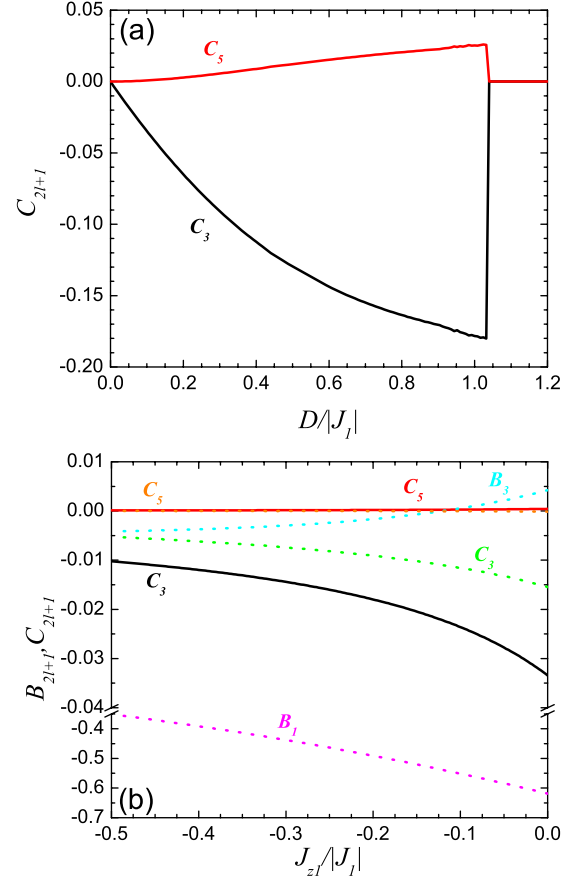
configurations may require more complex resolution functions.

III. MAGNETIC GROUND STATE

Using the intralayer exchange parameters estimated[22] for 3.5% Ga-doped $CuFeO_2$, we have evaluated the evolution of the spin harmonics with the interlayer interaction J_{z1}, anisotropy D, and lattice distortion K_1. The squares of the spin harmonics $(C_{2l+1})^2$ and $(B_{2l+1})^2$ are proportional to the ENS intensities at wave vectors $(2l+1)Q_x$ and $(2l+1)(2\pi-Q_x)$. Due to the antiferromagnetic coupling between planes, the observed ordering wave vector of $CuFeO_2$ is $\mathbf{Q}\approx(0.8\pi/a,0,\pi/c)$ or, with respect to the primitive unit cell, $[H,H,1.5]$ with $H\approx0.2$.

Without anisotropy or lattice distortion, the spin configuration is a simple spiral with ordering wave vector $\mathbf{Q}$. As shown in Fig. 2(a), Q_x decreases with the interlayer coupling J_{z1}. When anisotropy and lattice distortions are included, the spin harmonics create a CNC phase. As the harmonics evolve with increasing interlayer interaction, anisotropy, and lattice distortion, the turn angles become increasingly non-uniform and develop additional structure, as discussed be-
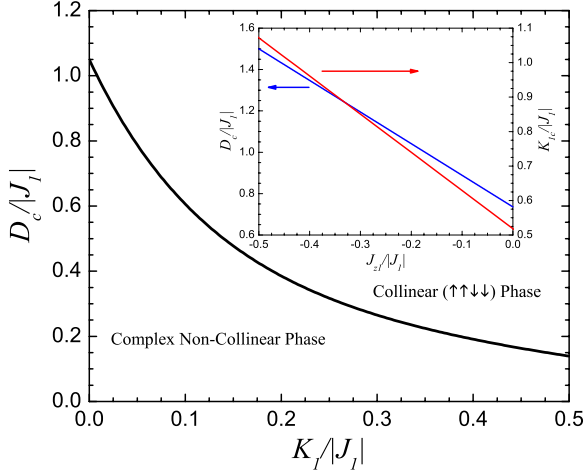
FIG. 4. (Color online) Critical anisotropy as a function of $K_1/|J_1|$ for $J_{z1}/|J_1|=-0.2$. The inset shows the critical anisotropy (left) and lattice distortion (right) as function of $J_{z1}/|J_1|$. The critical anisotropy is evaluated for $K_1/|J_1|=0$ while the critical lattice distortion is determined for $D/|J_1|=0.05$.

low. As shown in Fig. 2(b), Q_x increases with the anisotropy K_1. Above a threshold value of $K_1/|J_1|$, the noncollinear phase becomes energetically unstable and Q_x shifts to the value π for the $\uparrow\uparrow\downarrow\downarrow$ phase.

The solid lines in Fig. 3(a) plot the C_3 and C_5 coefficients as a function of the anisotropy with no lattice distortion. The value $J_{z1}/|J_1|=-0.2$ is used to demonstrate the effect of interlayer interactions on the spin harmonics. Below the critical value $D_c/|J_1|=1.03$, the CNC phase has lower energy than the $\uparrow\uparrow\downarrow\downarrow$ collinear phase. The inset of Fig. 4 shows that $D_c/|J_1|$ increases with $J_{z1}/|J_1|$. Hence, the antiferromagnetic interactions between layers tend to destabilize the collinear phase. Figure 3(b) demonstrates that the spin harmonics are reduced as $J_{z1}/|J_1|$ increases, implying that the spin state becomes less distorted as the interlayer interactions become more significant.

The B_{2l+1} harmonics are activated by the lattice distortion K_1, in qualitative agreement with the results of Zaliznyak[29] for a square lattice Heisenberg antiferromagnet with modulated interactions. Lattice distortions also reduce C_3 and C_5 and dramatically suppress the critical anisotropy, as shown in Fig. 4. Consequently, lattice distortions play an important role in stabilizing the $\uparrow\uparrow\downarrow\downarrow$ phase. With increasing $J_{z1}/|J_1|$, the dashed lines in Fig. 3(b) show a similar damping effect for the B_1 and B_3 harmonics.

Examining the spin harmonics as a function of $K_1/|J_1|$, we show in Fig. 5(a) that the B_1 harmonic dominates as the lattice distortion suppresses C_3 and C_5. Above the critical value $K_{1c}/|J_1|=0.73$, the system is pushed into the collinear $\uparrow\uparrow\downarrow\downarrow$ configuration. Figure 4(a) shows the evolution of K_{1c} with increasing J_{z1} and $D/|J_1|=0.05$.

To see how the CNC phase energetically compares to the proper spiral sketched in Fig. 1(c),[19,20] we plot the energy $E/|J_1|$ as function of $K_1/|J_1|$ in Fig. 5(b). The CNC phase is favored over both the $\uparrow\uparrow\downarrow\downarrow$ and proper configurations up to $K_{1c}/|J_1|=0.73$, above which the $\uparrow\uparrow\downarrow\downarrow$ configuration is stabilized. Without spin harmonics, the simple spiral is favored over the proper spiral.
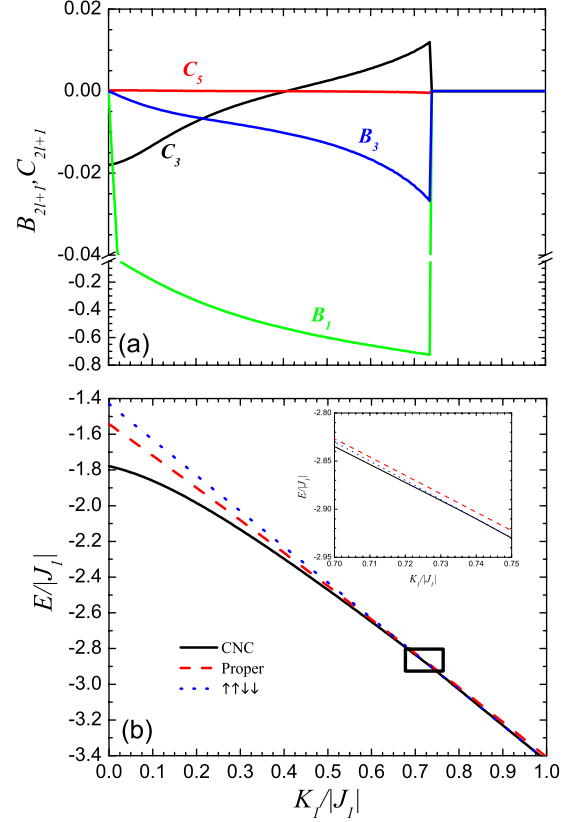

FIG. 5. (Color online) (a) The C_3, C_5, B_1, and B_3 spin harmonics as a function of $K_1/|J_1|$ for $D/|J_1|=0.05$ and $J_{z1}/|J_1|=-0.2$. (b) Energy as function of $K_1/|J_1|$ for the CNC, collinear, and proper spin configurations with $D/|J_1|=0.05$ and $J_{z1}/|J_1|=-0.2$.

Because the CNC phase is incommensurate and anharmonic, it contains turn angles $\Delta\theta$ that fluctuate around the averages $\overline{\Delta\theta_1}$ and $\overline{\Delta\theta_2}$. By contrast, a simple spiral contains only one turn angle $\Delta\theta$ [see Fig. 1(b)]. The proper spiral is obtained when $\Delta\theta_1=0$, which produces collinear zigzag chains. Unlike for the CNC phase, the turn angles of the proper spiral do not fluctuate around $\Delta\theta_1=0$ and $\Delta\theta_2$.

For 3.5% Ga-doped $CuFeO_2$, ENS measurements imply an average turn angle of 74°. Taking $\Delta\theta_1=0$, Nakajima et al.[19,20] therefore estimated that $\Delta\theta_2=152°$ for the proper spiral. Using interaction parameters determined from INS measurements, we found[22] that the turn angles for the CNC configuration fluctuate around $\overline{\Delta\theta_1}=22°$ and $\overline{\Delta\theta_2}=134°$, as shown in Fig. 1(d).

In Fig. 6(a), a nonuniform population density $\rho(\theta)$ of the spin angles θ is produced by the odd-order harmonics in the CNC phase. The distribution $\rho(\theta)$ peaks at $\theta=90°$ and 270° because the spins prefer to align along the z axis. For a simple spiral, $\rho(\theta)$ would be constant. The turn angles of the CNC configuration fluctuate about $\Delta\theta_1$ and $\Delta\theta_2$ due to the modulation created by the spin harmonics. The distribution $\rho(\Delta\theta)$ of turn angles $\Delta\theta$ for the CNC phase, plotted in Fig. 6(b), reveals a 6° variation about the average turn angles $\overline{\Delta\theta_1}=22°$ and $\overline{\Delta\theta_2}=134°$. Surprisingly, the distribution function $\rho(\Delta\theta)$ contains cusps at $\overline{\Delta\theta_n}\pm3°$.
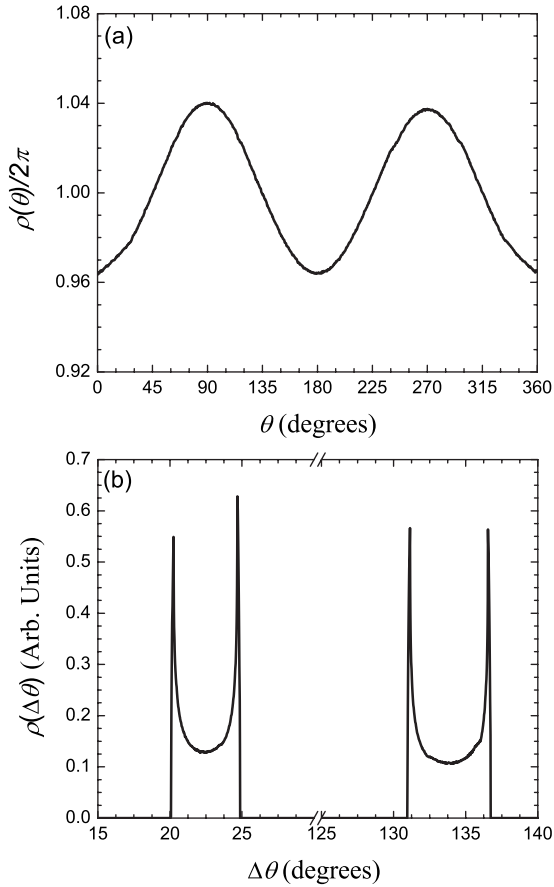
FIG. 6. (a) The population density of θ [rotation angle of **S** $=(0, S_y, S_z)$ from the y axis.] for the CNC phase. (b) The population density of the turn angles of the CNC phase with parameters taken from the third line in Table I.

IV. SPIN-WAVE DYNAMICS

To compliment the previous discussion, we have evaluated the SW dynamics for the simple spiral and CNC configurations. Because the proper spiral is not a stable spin configuration, it is impossible to evaluate its spin dynamics for comparison with the CNC results. Since the CNC phase was investigated[22] in 3.5% Ga-doped $CuFeO_2$, we will use those parameters to illustrate the effect of lattice distortions. We shall see that the INS spectra sensitively depends on the presence of spin harmonics in the ground state and provides a dynamical "fingerprint" of the CNC phase. Consequently, the SW dynamics can be used to identify the magnetic configuration of a material with competing interactions. Spin dynamics have also been shown to be vital in understanding the magnetic structure and properties of other materials.[37,38]

In order to evaluate the SW modes, we shall include not only the magnetic ground state with wavevector **Q** along the x direction but also the two twin ground states with wavevectors rotated in the xy plane by $\pm \pi/3$. While we shall assume that the crystal contains equal domains of all three states, lattice distortions may actually favor the growth of one state over the two twins.

Assuming no anisotropy and lattice distortion, the magnetic structure is a simple spiral [Fig. 1(b)] with a constant
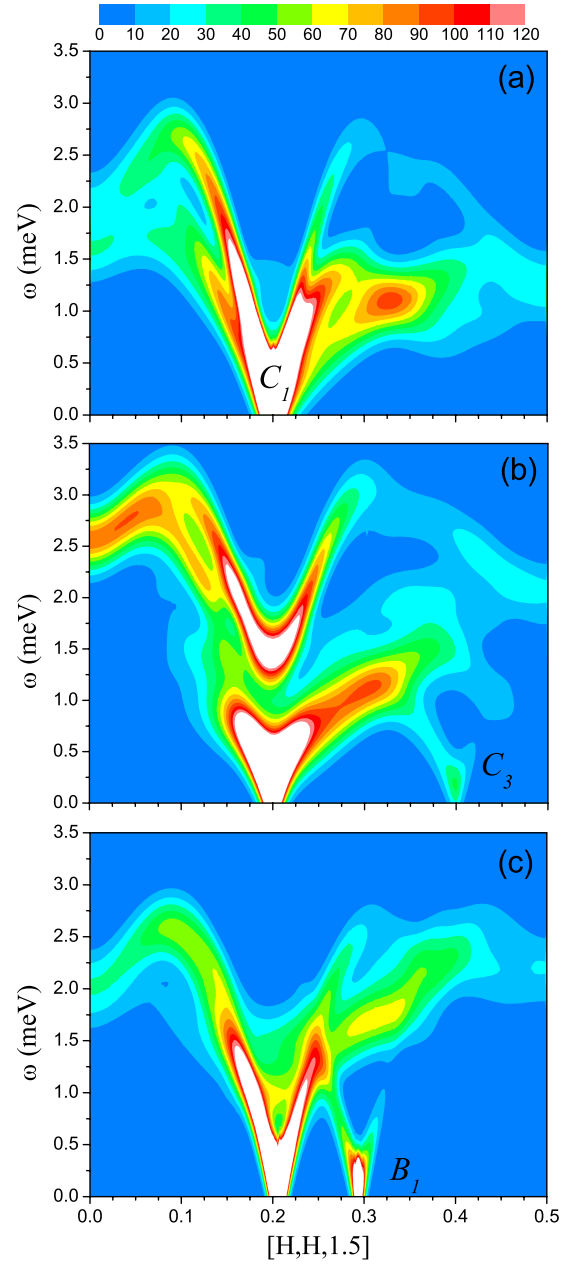

FIG. 7. (Color online) The predicted SW dynamics along $[H,H,1.5]$ incorporating intralayer and interlayer interactions: (a) the simple spiral without anisotropy and lattice distortion; (b) the CNC phase with $D/|J_1|=0.5$ and no lattice distortion; and (c) the CNC phase with $D/|J_1|=0.05$ and $K_1/|J_1|=0.35$.

turn angle of 74°. The SW dynamics along the $[H,H,0]$ direction in Fig. 7(a) reveals a single Goldstone mode at the ordering wavevector $H=0.2$ corresponding to this turn angle. Interlayer interactions produce the "shoulder" at low H. If no interlayer interactions were present, the SW frequency gap would vanish as $H \rightarrow 0$. Multiple SW modes are produced by the twin branches along $[H,0,0]$ and $[0,H,0]$. By doubling the unit cell, interlayer interactions create a second SW mode. All these factors combine to produce the complex dispersion shown.

With anisotropy $D/|J_1|=0.5$, a second Goldstone mode appears at $3Q_x$ or $H=0.4$. Associated with the C_3 harmonic,

TABLE I. Spin harmonics for spiral and CNC phases[a].

Phase (D, K_1) [b]	C_3	C_5	B_1	B_3	G_1
Simple (0.0,0.0)	0.0	0.0	0.0	0.0	0.0
CNC (0.1, 0.0)	−0.12	−0.011	0.0	0.0	0.0
CNC (0.01, 0.07)	-8.4×10^{-4}	-4.0×10^{-5}	−0.52	−0.011	0.51

[a]C_1 is set to 1. For all cases $Q_x \approx 0.84\pi/a$.

[b]D and K_1 are given in meV.

this mode is about an order of magnitude lower in intensity than the mode associated with the C_1 harmonic. Since the mode associated with the C_5 harmonic is about two orders of magnitude lower in intensity, it is not observable. Because anisotropy raises the second SW mode at the ordering wavevector, it is possible to estimate the anisotropy of the CNC phase from the SW spectra.

Figure 7(c) plots the predicted SW dynamics with $K_1/|J_1|=0.35$ and $D/|J_1|=0.05$. Lattice distortions activate the B_1 harmonic at $2\pi-Q_x$ or $H=0.3$. Due to the large value of B_1, the intensity of the secondary peak at $H=0.3$ has about 25% of the intensity of the main peak at $H=0.2$. Since lattice distortions weaken the C_3 harmonic, the $3Q_x$ mode at $H=0.4$ is no longer observable. The harmonics presented in Table I are used to produce a CNC spin configuration with turn angles that fluctuate around 22° and 134° with an average turn angle of about 76°. These results were recently used to describe the INS measurements[22] for 3.5% Ga-doped CuFeO$_2$ and confirm the magnetic structure of the multiferroic phase.

By comparing the SW dispersions in Fig. 7 with experimental measurements, we have been able to isolate the separate roles of anisotropy and lattice distortions in the magnetic structure of doped CuFeO$_2$.[22] While ENS can help determine the harmonics of the spin configuration, only INS measurements allowed us to determine the exchange interactions and magnetic structure of the ground state.

The overall interaction values estimated for doped CuFeO$_2$ are slightly lower than those for pure CuFeO$_2$ due to the disruption of the exchange pathways by Ga doping. The main difference between the undoped and doped samples is the dramatic decrease in the anisotropy D for the latter. This reduction is consistent with predicted effects of Al doping.[15] It should be mentioned that the fit of the SW spectrum for the undoped sample[25] did not include lattice distortions which were properly included in the fits for the doped sample.[39] The lattice distortion would have most likely reduced the fitted value for the anisotropy in the undoped sample.

V. CONCLUSION

This paper has investigated the effect of interlayer interactions and lattice distortions on the magnetic ground state and spin dynamics for a geometrically frustrated triangular-lattice antiferromagnet. Lattice distortions produce a CNC phase that is energetically favored over both simple and proper spirals.[20] The simple incommensurate spiral is distorted by anisotropy and the spins favor the $\pm z$ directions. While weakening the C_3 and C_5 harmonics at $3Q_x$ and $5Q_x$, lattice distortions activate the B_1 harmonic at $2\pi-Q_x$. Lattice distortions in Ga-doped or Al-doped CuFeO$_2$ may be sufficiently large that the C_3 harmonic has not yet been observed in ENS measurements.

Using a Holstein-Primakoff expansion, we evaluated the evolution of the SW dynamics about the simple spiral and CNC states. Anisotropy and lattice distortions produce extra Goldstone modes at $3Q_x$ and $2\pi-Q_x$. The complexity of the INS spectrum and the detailed agreement with theoretical predictions[22] allows us to unambiguously identify the CNC phase with the multiferroic phase in doped CuFeO$_2$.

In principle, ENS measurements alone should be adequate to extract all the spin harmonics and identify the spin ground state. However, the ground state of doped CuFeO$_2$ is sufficiently complex and the higher spin harmonics are insufficiently strong to allow ENS measurements to distinguish between candidate ground states including the proper spiral. This paper has shown that INS measurements provide a dynamical fingerprint that allows us to identify the complex magnetic ground state of Ga-doped CuFeO$_2$. This methodology should also be useful in the identification of the magnetic structure in other frustrated magnetic materials[23,24] such as CuCrO$_2$ and MnWO$_4$.

[1] T. Kimura, T. Goto, H. Shintani, K. Ishizaka, T. Arima, and Y. Tokura, Nature (London) **426**, 55 (2003).

[2] D. I. Khomskii, J. Magn. Magn. Mater. **306**, 1 (2006).

[3] S.-W. Cheong and M. Mostovoy, Nature Mater. **6**, 13 (2007).

[4] R. Ramesh and N. A. Spaldin, Nature Mater. **6**, 21 (2007).

[5] W. Eerenstein, N. D. Mathur, and J. F. Scott, Nature (London) **442**, 759 (2006).

[6] M. Mostovoy, Phys. Rev. Lett. **96**, 067601 (2006).

[7] T. Arima, J. Phys. Soc. Jpn. **76**, 073702 (2007).

[8] See, for example, *Frustrated Spin Systems*, edited by H. T. Diep (World Scientific, New Jersey, 2004).

[9] S. Mitsuda, H. Yoshizawa, N. Yaguchi, and M. Mekata, J. Phys. Soc. Jpn. **60**, 1885 (1991).

[10] S. Mitsuda, M. Mase, K. Prokes, H. Kitazawa, and H. Aruga Katori, J. Phys. Soc. Jpn. **69**, 3513 (2000).

[11] N. Terada, S. Mitsuda, T. Fujii, and D. Petitgrand, J. Phys.: Condens. Matter **19**, 145241 (2007).

[12] F. Ye, J. A. Fernandez-Baca, R. S. Fishman, Y. Ren, H. J. Kang, Y. Qiu, and T. Kimura, Phys. Rev. Lett. **99**, 157201 (2007).

[13] N. Terada, S. Mitsuda, T. Fujii, K. Soejima, I. Doi, H. A. Katori, and Y. Noda, J. Phys. Soc. Jpn. **74**, 2604 (2005).

[14] S. Seki, Y. Yamasaki, Y. Shiomi, S. Iguchi, Y. Onose, and Y. Tokura, Phys. Rev. B **75**, 100403(R) (2007).

[15] R. S. Fishman, J. Appl. Phys. **103**, 07B109 (2008).

[16] M. Swanson, J. T. Haraldsen, and R. S. Fishman, Phys. Rev. B **79**, 184413 (2009).

[17] J. T. Haraldsen, M. Swanson, G. Alvarez, and R. S. Fishman, Phys. Rev. Lett. **102**, 237204 (2009).

[18] N. Terada, T. Nakajima, S. Mitsuda, H. Kitazawa, K. Kaneko, and N. Metoki, Phys. Rev. B **78**, 014101 (2008).

[19] T. Nakajima, S. Mitsuda, S. Kanetsuki, K. Prokes, A. Podlesnyak, H. Kimura, and Y. Noda, J. Phys. Soc. Jpn. **76**, 043709 (2007).

[20] T. Nakajima, S. Mitsuda, K. Takahashi, M. Yamano, K. Masuda, H. Yamazaki, K. Prokes, K. Kiefer, S. Gerischer, N. Terada, H. Kitazawa, M. Matsuda, K. Kakurai, H. Kimura, Y. Noda, M. Soda, M. Matsuura, and K. Hirota, Phys. Rev. B **79**, 214423 (2009).

[21] R. S. Fishman and S. Okamoto, Phys. Rev. B **81**, 020402(R) (2010).

[22] J. T. Haraldsen, F. Ye, R. S. Fishman, J. A. Fernandez-Baca, Y. Yamaguchi, K. Kimura, and T. Kimura, Phys. Rev. B **82**, 020404(R) (2010).

[23] S. Seki, Y. Onose, and Y. Tokura, Phys. Rev. Lett. **101**, 067204 (2008); M. Poienar, F. Damay, C. Martin, J. Robert, and S. Petit, Phys. Rev. B **81**, 104411 (2010).

[24] A. H. Arkenbout, T. T. M. Palstra, T. Siegrist, and T. Kimura, Phys. Rev. B **74**, 184431 (2006); K. Taniguchi, N. Abe, T. Takenobu, Y. Iwasa, and T. Arima, Phys. Rev. Lett. **97**, 097203 (2006).

[25] R. S. Fishman, F. Ye, J. A. Fernandez-Baca, J. T. Haraldsen, and T. Kimura, Phys. Rev. B **78**, 140407(R) (2008).

[26] N. Terada, S. Mitsuda, H. Ohsumi, and K. Tajima, J. Phys. Soc. Jpn. **75**, 023602 (2006).

[27] N. Terada, Y. Tanaka, Y. Tabata, K. Katsumata, A. Kikkiawa, and S. Mitsuda, J. Phys. Soc. Jpn. **75**, 113702 (2006).

[28] T. Nakajima, S. Mitsuda, T. Inami, N. Terada, H. Ohsumi, K. Prokes, and A. Podlesnyak, Phys. Rev. B **78**, 024106 (2008).

[29] I. A. Zaliznyak, Phys. Rev. B **68**, 134451 (2003); **69**, 092404 (2004).

[30] J. T. Haraldsen and R. S. Fishman, J. Phys.: Condens. Matter **21**, 216001 (2009).

[31] M. E. Zhitomirsky and I. A. Zaliznyak, Phys. Rev. B **53**, 3428 (1996).

[32] G. L. Squires, *Introduction to the Theory of Thermal Neutron Scattering* (Dover, New York, 1978).

[33] G. Shirane, S. M. Shapiro, and J. M. Tranquada, *Neutron Scattering with a Triple-Axis Spectrometer* (Cambridge University Press, Cambridge, 2002).

[34] The Fe^{3+} magnetic form factor is given as $F_{\mathbf{q}} = j_0(\mathbf{q})$, where $j_0(\mathbf{q}) = A_0 e^{a_0 s^2} + B_0 e^{b_0 s^2} + C_0 e^{c_0 s^2} + D_0$ and $s = \sin\theta/\lambda = q/4\pi$. The coefficients are $A_0 = 0.3972$ ($a_0 = 13.2442$), $B_0 = 0.6295$ ($b_0 = 4.9034$), $C_0 = -0.0314$ ($c_0 = 0.3496$), and $D_0 = 0.0044$ from Ref. 35.

[35] A. J. Dianoux and G. Lander, *Neutron Data Booklet* (OCP Science, Philadelphia, 2003).

[36] N. J. Chesser and J. D. Axe, Acta Crystallogr., Sect. A: Cryst. Phys., Diffr., Theor. Gen. Crystallogr. **29**, 160 (1973).

[37] A. W. Garrett, S. E. Nagler, D. A. Tennant, B. C. Sales, and T. Barnes, Phys. Rev. Lett. **79**, 745 (1997).

[38] B. Skubic, O. E. Peil, J. Hellsvik, P. Nordblad, L. Nordström, and O. Eriksson, Phys. Rev. B **79**, 024411 (2009).

[39] For the doped sample, the parameters were manually adjusted to fit the data because the data sets consist of multiple three-dimensional matrices. This is different from the numerical least squares fitting used to analyze the undoped sample (Ref. 25).